Effect of Channel Estimation Error on M-QAM BER Performance in Rayleigh Fading

Xiaoyi Tang, Mohamed-Slim Alouini, *Member, IEEE,* and Andrea J. Goldsmith, *Senior Member, IEEE*

***Abstract*—We determine the bit-error rate (BER) of multilevel quadrature amplitude modulation (M-QAM) in flat Rayleigh fading with imperfect channel estimates. Despite its high spectral efficiency, M-QAM is not commonly used over fading channels because of the channel amplitude and phase variation. Since the decision regions of the demodulator depend on the channel fading, estimation error of the channel variation can severely degrade the demodulator performance. Among the various fading estimation techniques, pilot symbol assisted modulation (PSAM) proves to be an effective choice. We first characterize the distribution of the amplitude and phase estimates using PSAM. We then use this distribution to obtain the BER of M-QAM as a function of the PSAM and channel parameters. By using a change of variables, our exact BER expression has a particularly simple form that involves just a few finite-range integrals. This approach can be used to compute the BER for any value of M. We compute the BER for 16-QAM and 64-QAM numerically and verify our analytical results by computer simulation. We show that for these modulations, amplitude estimation error leads to a 1-dB degradation in average signal-to-noise ratio and combined amplitude-phase estimation error leads to 2.5-dB degradation for the parameters we consider.**

***Index Terms*— Channel estimation error, M-QAM, PSAM, Rayleigh fading.**

I. Introduction

DUE TO its high spectral efficiency, multilevel quadrature amplitude modulation (M-QAM) is an attractive modulation technique for wireless communications. M-QAM has been recently proposed and studied for various nonadaptive [1]–[3] and adaptive [4], [5] wireless systems. However, the severe amplitude and phase fluctuations inherent to wireless channels significantly degrade the bit-error rate (BER) performance of M-QAM. That is because the demodulator must scale the received signal to normalize channel gain so that its decision regions correspond to the transmitted signal constellation. This scaling process is called automatic gain control (AGC) [6]. If the channel gain is estimated in error, then the AGC improperly scales the received signal, which can lead to incorrect demodulation even in the absence of noise. Thus, reliable communication with M-QAM requires accurate fading compensation techniques at the receiver.

Channel sounding in M-QAM demodulation is a very effective technique to precisely compensate for channel amplitude and phase distortion. Channel sounding by pilot symbol assisted modulation (PSAM) has been studied by several authors [7]–[10] and proven to be effective for Rayleigh fading channels. Previous studies on the performance of M-QAM with PSAM were primarily based on computer simulation and experimental implementation [7], [9], [10]. The only analytical result is a tight upper bound on the symbol-error rate for 16-QAM [8]. These results do not provide an easy method to evaluate the performance tradeoffs for different system design parameters.

Some work has been done on the AGC error problem based on various models [11], [12]. In [11], a simple model has the fading estimate $\hat{\gamma}$ related to the fading γ by a single parameter $\varepsilon_{\mathrm{AGC}}$: $\hat{\gamma} = \bar{\gamma}\varepsilon_{\mathrm{AGC}} + \gamma(1 - \varepsilon_{\mathrm{AGC}})$, where $\bar{\gamma}$ is the average value of the fading. When $\varepsilon_{\mathrm{AGC}}$ is 0, $\hat{\gamma} = \gamma$, which corresponds to perfect AGC. When $\varepsilon_{\mathrm{AGC}}$ is 1, $\hat{\gamma} = \bar{\gamma}$, corresponding to no AGC. Imperfect AGC is modeled by appropriate values of $\varepsilon_{\mathrm{AGC}}$. However, this model cannot be used to determine the performance of M-QAM using PSAM because the PSAM parameters cannot be mapped to $\varepsilon_{\mathrm{AGC}}$. In [12], the authors obtain the distribution of a "final noise" that includes the multiplicative fading distortion due to imperfect AGC as well as additive white Gaussian noise (AWGN). Even though the approach in [12] is valid for any linearly modulated signal over flat Ricean fading channels, no explicit BER expression is given for M-QAM with channel estimation error.

In this paper, we provide a general approach to calculate the exact BER of M-QAM with PSAM in flat Rayleigh fading channels. In particular, we derive the exact BER of 16-QAM and 64-QAM using PSAM. These BER expressions are given by a few finite-range integrals, which are easy to calculate numerically using standard mathematical packages such as Mathematica. The BER of M-QAM with larger constellation sizes can be derived in a similar manner. We also obtain the BER using computer simulations, and these simulated results match closely with those obtained from our analysis.

The remainder of this paper is organized as follows. In Section II, we outline the communication system and channel models. In Section III, we describe the PSAM system and derive two parameters later used in the BER expression of

Paper approved by K. B. Letaief, the Editor for Wireless Systems of the IEEE Communications Society. Manuscript received November 2, 1998; revised March 15, 1999 and May 27, 1999. This work was supported in part by NSF CAREER Development Award NCR-9501452. The work of X. Tang was supported by a Caltech Summer Undergraduate Research Fellowship. This paper was presented in part at the 1999 IEEE Vehicular Technology Conference, Houston, TX, May 1999.

X. Tang is with the Department of Electrical Engineering and Computer Science, University of California, Berkeley, CA 94705 USA (e-mail: xiaoyi @eecs.berkeley.edu).

M.-S. Alouini is with the Department of Electrical and Computer Engineering, University of Minnesota, Minneapolis, MN 55455 USA (e-mail: alouini@ece.umn.edu).

A. J. Goldsmith is with the Department of Electrical Engineering, Stanford University, Stanford, CA 94305-9515 USA (e-mail: andrea@ee.stanford.edu).

Publisher Item Identifier S 0090-6778(99)09776-7.

TABLE I
LIST OF SYMBOLS

α, θ	fading amplitude and phase, respectively
$\hat{\alpha}$, $\hat{\theta}$	estimates of α and θ, respectivel y
Ω, $\hat{\Omega}$	E$\{\alpha^2\}$ and E$\{\hat{\alpha}^2\}$, respectively
ρ	correlation coefficient between α^2 and $\hat{\alpha}^2$
r	$\hat{\Omega}/\Omega$
K	interpolation size for PSAM interpolator
L	frame size L
$\overline{\gamma}$	average signal to noise ratio per symbol ($\Omega E_s/N_o$)
$\overline{\gamma_b}$	average signal to noise ratio per bit ($\Omega E_b/N_o$)
$f_d T_s$	normalized Doppler spread

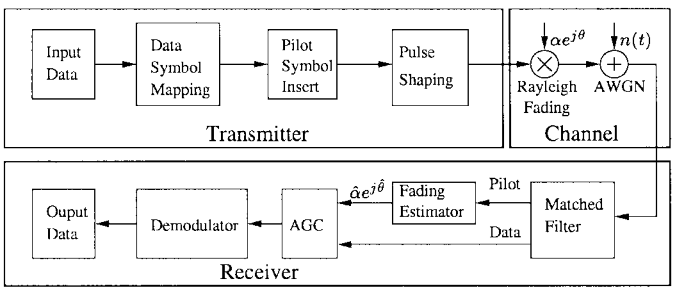

Fig. 1. System block diagram.

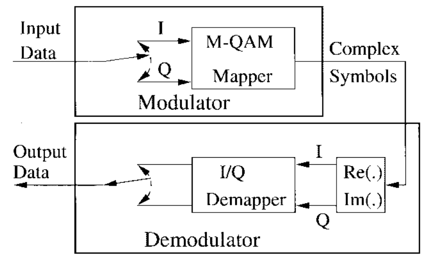

Fig. 2. M-QAM: modulation and demodulation.

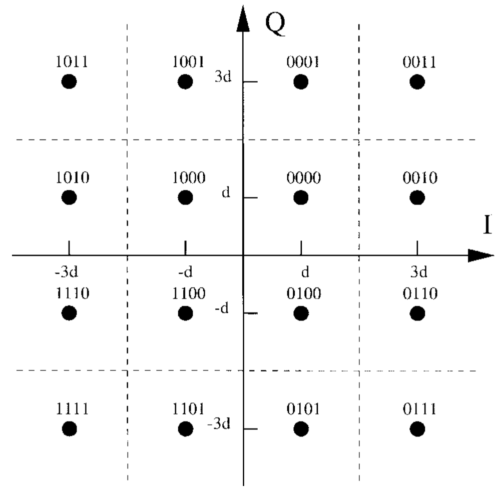

Fig. 3. 16-QAM constellation with Gray encoding.

M-QAM. In Section IV, we derive the exact BER of M-QAM with imperfect AGC. We start with conditional BER and obtain the final BER in terms of finite-range integrals. We first consider the amplitude estimation error only and then go on to include both the amplitude and the phase estimation errors. Numerical BER results from both analysis and simulation are also presented in this section.

For reference, Table I summarizes the symbols we use to represent key parameters throughout the paper.

II. SYSTEM AND CHANNEL MODELS

A block diagram of the PSAM communication system is shown in Fig. 1. Pilot symbols are periodically inserted into the data symbols at the transmitter so that the channel-induced envelope fluctuation α and phase shift θ can be extracted and interpolated at the channel estimation stage. These estimates are given by $\hat{\alpha}$ and $\hat{\theta}$, respectively. The received signal goes through the AGC, which compensates for the channel fading by dividing the received signal by the fading estimate $\hat{\alpha}e^{j\hat{\theta}}$. The output from the AGC is then fed to the decision device to obtain the demodulated data bits.

We assume a slowly-varying flat-fading Rayleigh channel at a rate slower than the symbol rate, so that the channel remains roughly constant over each symbol duration. The Rayleigh fading amplitude α follows the probability density function (pdf)

$$p(\alpha) = \frac{2\alpha}{\Omega} e^{-(\alpha^2/\Omega)}, \qquad \alpha > 0 \tag{1}$$

where $\Omega = E\{\alpha^2\}$ is the average fading power. The joint distributions $p(\alpha, \hat{\alpha})$ and $p(\theta, \hat{\theta})$ will be derived in Section III-A, after we describe the details of PSAM.

Fig. 2 shows the modulation and demodulation of square M-QAM. At the modulator, the data bit stream is split into the inphase (I) and quadrature (Q) bit streams. The I and Q components together are mapped to complex symbols using Gray coding. The demodulator splits the complex symbols into I and Q components and puts them into a decision device (demapper), where they are demodulated independently against their respective decision boundaries. Demodulation of the I and Q bit streams is identical due to symmetry. Average BER of M-QAM is then equal to the BER of either the I or the Q component. Figs. 3 and 4 show the constellation, decision boundaries, and bit-mapping for square 16-QAM and square 64-QAM, respectively [1]. For 16-QAM, the first and third bits are passed to the inphase bit stream, while the second and fourth bits are passed to the quadrature bit stream. The separate I and Q components are then each Gray-encoded by assigning the bits 01, 00, 10, and 11 to the levels $3d$, d, $-d$, and $-3d$, respectively, as shown by the first line in Fig. 5. In our BER calculation, we will compute the BER for each bit separately. Thus, we need the individual decision regions for each bit. In Fig. 5, the decision region boundaries for the most significant bit (MSB) and the least significant bit (LSB) are shown in lines 2 and 3, respectively, where MSB and LSB refer to the left and right bits, respectively, in the first line of the figure. For 64-QAM, the first, third, and fifth bits are passed to the inphase bit stream, while the remaining bits are passed to the quadrature bit stream. These individual I and Q components are then each Gray-encoded by assigning the bits 011, 010, 000, 001, 101, 100, 110, and 111 to the levels $7d$,

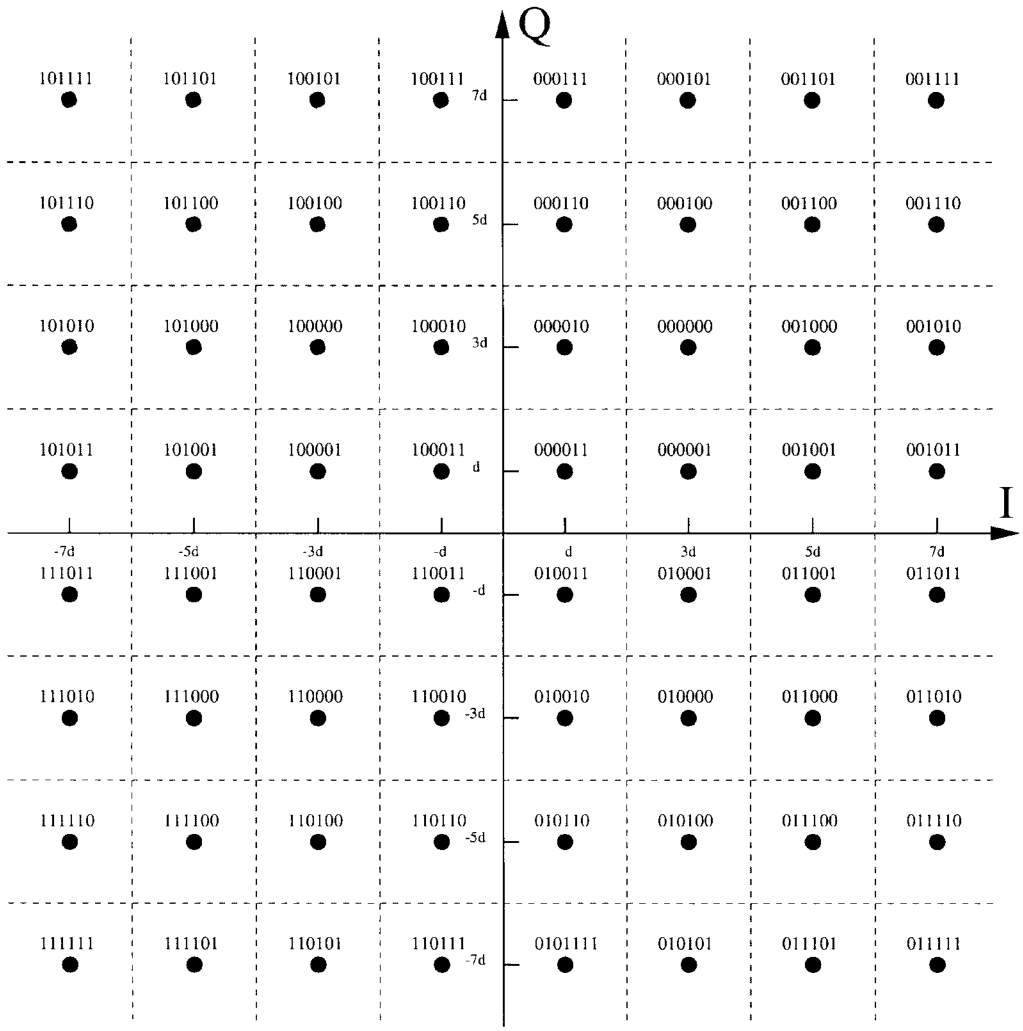

Fig. 4. 64-QAM constellation with Gray encoding.

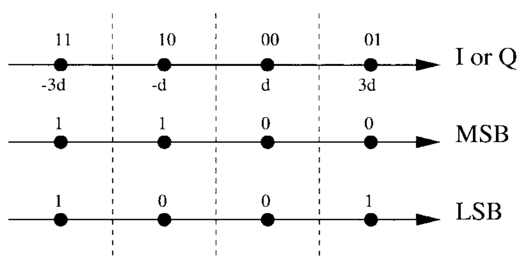

Fig. 5. 16-QAM bit-by-bit demapping.

$5d$, $3d$, $1d$, $-d$, $-3d$, $-5d$, and $-7d$, respectively, as shown by the first line in Fig. 6. In this figure, the second, third, and fourth lines show the decision region boundaries for the MSB, mid bit, and LSB corresponding to the left bit, the middle bit, and the right bit, respectively, in the first line of the figure. The decision regions for demodulation (demapping) of either the I or the Q component and its corresponding bits are shown in Figs. 5 and 6 for 16-QAM and 64-QAM, respectively. Although our calculations below only apply to symmetrical M-QAM constellations with Gray bit mapping, our methods can be extended to nonsymmetrical constellations and other bit mappings that can be decomposed into I and Q components.

III. PSAM

A. PSAM System Description

References [7], [9], and [10] provide detailed descriptions of the PSAM method. In short, pilot symbols are periodically inserted into the data symbols to estimate the fading. Specifically, the data is formatted into frames of L symbols, with the first symbol in each frame used for the pilot symbol, as shown in Fig. 7.

After matched filtering and sampling with perfect symbol timing at the rate of $1/T_s$, a baseband T_s-spaced discrete-time complex-valued signal is obtained as

$$r_k = z_k a_k + n_k. \tag{2}$$

The sequence a_k represents complex M-QAM and pilot symbols. The sequence z_k represents the fading, which for Rayleigh channels, is a complex zero-mean Gaussian random variable, and n_k is AWGN with variance $\sigma_n^2 = N_o/2$. At the receiver, channel fading at the pilot symbol times is extracted by dividing the received signal by the known pilot symbols denoted by a

$$\hat{z}_i = \frac{r_i}{a} = z_i + \frac{n_i}{a} \tag{3}$$

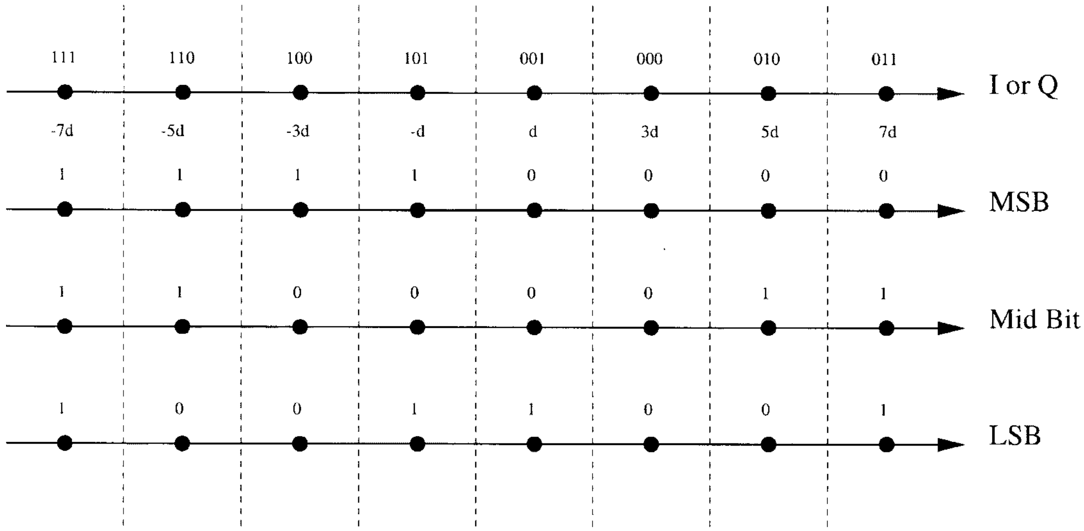

Fig. 6. 64-QAM bit-by-bit demapping.

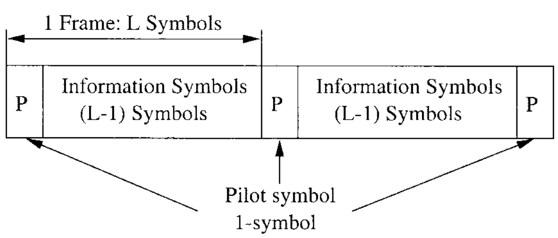

Fig. 7. Frame format.

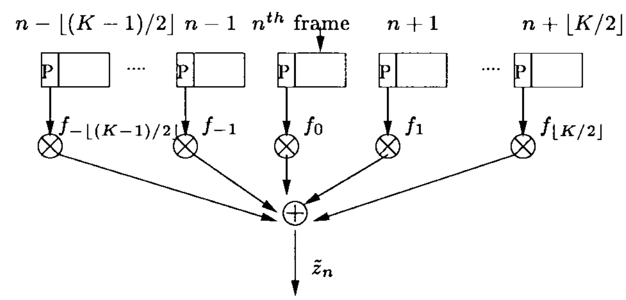

Fig. 8. Fading interpolation in PSAM.

where z_i is the fading at the pilot symbol in the ith frame. The receiver estimates the fading at the lth data symbol time in the nth frame from the K nearest pilot symbols, i.e., the receiver uses $\lfloor (K-1)/2 \rfloor$ pilot symbols from previous frames, the pilot symbol from the current frame, and the pilot symbols from the $\lfloor K/2 \rfloor$ subsequent frames, as illustrated in Fig. 8. Thus, the fading estimate is given by

$$\tilde{z}_n^l = \sum_{k=-\lfloor (K-1)/2 \rfloor}^{\lfloor K/2 \rfloor} f_k^l \hat{z}_{n+k} \tag{4}$$

where $l = 1, \cdots, L-1$ is the data symbol index within each frame, and f_k^l are real numbered interpolation coefficients, as we explain in more detail in Section III-C.

Since the estimated fading $\tilde{z}$ is a weighted sum of zero-mean complex Gaussian random variables, it is also a zero-mean complex Gaussian random variable. Thus, the amplitude $\alpha = |z|$ and its estimate $\hat{\alpha} = |\tilde{z}|$ have a bivariate Rayleigh distribution given by

$$p(\alpha, \hat{\alpha}) = \frac{4\alpha\hat{\alpha}}{(1-\rho)\Omega\hat{\Omega}} I_0\left(\frac{2\sqrt{\rho}\alpha\hat{\alpha}}{(1-\rho)\sqrt{\Omega\hat{\Omega}}}\right) \cdot \exp\left[-\frac{1}{1-\rho}\left(\frac{\alpha^2}{\Omega} + \frac{\hat{\alpha}^2}{\hat{\Omega}}\right)\right] \tag{5}$$

where $\rho = ((\mathrm{cov}(\alpha^2, \hat{\alpha}^2))/(\sqrt{\mathrm{var}(\alpha^2)\mathrm{var}(\hat{\alpha^2})}))$, $0 \le \rho < 1$, is the correlation coefficient between α^2 and $\hat{\alpha}^2$, $\Omega = E\{\alpha^2\}$, $\hat{\Omega} = E\{\hat{\alpha}^2\}$, and $I_0(\cdot)$ is the zeroth-order modified Bessel function. The phase θ and its estimate $\hat{\theta}$ have a joint distribution similar to [13, eq. (8.106)] given by

$$p(\theta, \hat{\theta}) = \frac{1-\rho}{4\pi^2}\left[\frac{(1-q^2)^{1/2} + q(\pi - \cos^{-1} q)}{(1-q^2)^{3/2}}\right], \quad 0 \le \theta, \quad \hat{\theta} \le 2\pi \tag{6}$$

where $q = \sqrt{\rho}\cos(\theta - \hat{\theta})$ and ρ is the same as that in (5).

B. Derivation of ρ and $r = (\hat{\Omega}/\Omega)$

The joint distribution of α and $\hat{\alpha}$ given by (5) contains three parameters: ρ, Ω, and $\hat{\Omega}$. The parameter ρ also appears in the joint distribution of θ and $\hat{\theta}$ given by (6). It turns out that ρ and $r = (\hat{\Omega}/\Omega)$ are needed in the final BER expression. For PSAM, these parameters can be expressed in closed form in terms of the PSAM and channel parameters, namely the interpolation size K, frame size L, average signal-to-noise ratio (SNR), and normalized Doppler spread $f_d T_s$.

The complex fading can be expressed as $z(t) = x(t) + jy(t)$. For Rayleigh channels, $x(t)$ and $y(t)$ are zero-mean independent Gaussian random processes, with autocorrelation and cross-correlation functions given by [14]

$$\begin{aligned} R_{xx}(\tau) &= E\{x(t)x(t+\tau)\} = R_{yy}(\tau) = E\{y(t)y(t+\tau)\} \\ &= R(\tau) = \frac{\Omega}{2} J_0(2\pi f_d \tau) \\ R_{xy}(\tau) &= E\{x(t)y(t+\tau)\} = 0. \end{aligned} \tag{7}$$

For $kT_s \le t < (k+1)T_s$, $z_k = x_k + jy_k$. Define the $K \times K$ covariance matrix $\mathbf{R}$ as

$$R_{mn} = \frac{1}{2}\,\mathrm{cov}(z_m, z_n^*). \tag{8}$$

Using (7), it can be shown that

$$\begin{aligned} R_{mn} &= \frac{1}{2}E\{(x_m + jy_m)(x_n - jy_n)\} \\ &= \frac{1}{2}(E\{x_m x_n\} + E\{y_m y_n\}) \\ &= R(\tau_{mn}) \end{aligned} \tag{9}$$

where τ_{mn} is the time difference between fading at two pilot symbols z_m and z_n

$$\tau_{mn} = |m-n|LT_s \tag{10}$$

with L the frame size and T_s the symbol duration.

We now obtain expressions for r and the correlation coefficient ρ in terms of the PSAM and channel parameters. From (3) and (4)

$$\begin{aligned} \tilde{z}_n^l &= \sum_{k=-\lfloor (K-1)/2\rfloor}^{\lfloor K/2\rfloor} f_k^l \hat{z}_{n+k} \\ &= \sum f_k\Big(x_k + \frac{n_{Ik}}{a}\Big) + j\sum f_k\Big(y_k + \frac{n_{Qk}}{a}\Big). \end{aligned} \tag{11}$$

Note that in the right-hand side of the above equation, the indices l and n are dropped for simplicity of notation since $\tilde{z}_n^l$ is a stationary process. Thus, $\hat{\alpha} = |\tilde{z}|$ is also Rayleigh distributed, with average power

$$\begin{aligned} \hat{\Omega} &= 2\,\mathrm{var}\left(\sum_{k=-\lfloor (K-1)/2\rfloor}^{\lfloor K/2\rfloor} f_k\Big(x_k + \frac{n_{Ik}}{a}\Big)\right) \\ &= 2\sum_k\sum_m f_k f_m\,\mathrm{cov}(x_k, x_m) + 2\sum_k \frac{f_k^2\sigma_n^2}{a^2} \\ &= 2\mathbf{FRF}' + 2\frac{\sigma_n^2}{a^2}|\mathbf{F}|^2 \end{aligned} \tag{12}$$

where $\mathbf{F} = [f_{-\lfloor (K-1)/2\rfloor}, \cdots, f_{\lfloor K/2\rfloor}]$ is a row vector and $\sigma_n^2 = \mathrm{var}(n_{Ik}) = \mathrm{var}(n_{Qk}) = (N_o/2)$ is the noise variance.

Hence

$$r = \frac{\hat{\Omega}}{\Omega} = \frac{2\mathbf{FRF}' + 2\frac{\sigma_n^2}{a^2}|\mathbf{F}|^2}{\Omega} = \mathbf{FR^0F}' + 2\frac{\sigma_n^2}{a^2\Omega}|\mathbf{F}|^2 \tag{13}$$

where $\mathbf{R^0} = (2/\Omega)\mathbf{R}$ is the normalized covariance matrix. Consider the case where the pilot symbol energy is equal to the average data symbol energy E_s. Thus

$$2\frac{\sigma_n^2}{a^2\Omega} = \frac{N_o}{E_s\Omega}. \tag{14}$$

Let us define the average SNR per symbol $\bar{\gamma}$ as

$$\bar{\gamma} = \frac{\Omega E_s}{N_o} = \frac{\Omega E_b \log_2 M}{N_o}. \tag{15}$$

The corresponding average SNR per bit is then $\overline{\gamma_b} = \bar{\gamma}/\log_2 M = \Omega E_b/N_o$. Then

$$r = \mathbf{FR^0F}' + \frac{|\mathbf{F}|^2}{\bar{\gamma}}. \tag{16}$$

Since α and $\hat{\alpha}$ follow the Rayleigh pdf as given by (1), it is easily shown that the standard deviations of α^2 and $\hat{\alpha}^2$ are Ω and $\hat{\Omega}$, respectively. Moreover, the covariance between α^2 and $\hat{\alpha}^2$ is given by (17), shown at the bottom of the page. Thus

$$\begin{aligned} \rho &= \frac{\mathrm{cov}(\alpha^2, \hat{\alpha}^2)}{\sqrt{\mathrm{var}(\alpha^2)\,\mathrm{var}(\hat{\alpha}^2)}} \\ &= \frac{4\left(\sum_k f_k E\{xx_k\}\right)^2}{\Omega\hat{\Omega}} \\ &= \frac{\bar{\gamma}\left(\sum_k f_k R^0(\tau_k)\right)^2}{\bar{\gamma}\mathbf{FR^0F}' + |\mathbf{F}|^2} \end{aligned} \tag{18}$$

where

$$R^0(\tau_k) = \frac{2E\{xx_k\}}{\Omega} = J_0(2\pi f_d \tau_k) \tag{19}$$

is the normalized covariance between the fading at data symbol z_n^l and at pilot symbol z_{k+n}, and $\tau_k = (k\,L + l)T_s$. Since the estimation coefficients and $R^0(\tau_k)$ depend on the position (l) within a frame, r and ρ need to be averaged over each data symbol position within a frame.

$$\begin{aligned} \mathrm{cov}\big(\alpha^2, \hat{\alpha}^2\big) &= E\big\{\alpha^2\hat{\alpha}^2\big\} - E\big\{\alpha^2\big\}E\big\{\hat{\alpha}^2\big\} \\ &= E\left\{zz^*\left(\sum_{k=-\lfloor (K-1)/2\rfloor}^{\lfloor K/2\rfloor} f_k\hat{z}_k\right)\left(\sum_{k=-\lfloor (K-1)/2\rfloor}^{\lfloor K/2\rfloor} f_k\hat{z}_k\right)^*\right\} - \Omega\hat{\Omega} \\ &= E\left\{\big(x^2+y^2\big)\sum_k\sum_m f_k f_m\left[x_k x_m + y_k y_m + j(x_m y_k - x_k y_m) + \frac{n_k n_m^*}{a^2}\right]\right\} - \Omega\hat{\Omega} \\ &= \frac{2\sigma_n^2\Omega}{a^2}|\mathbf{F}|^2 + 2\Omega\mathbf{FRF}' + 4\left(\sum_k f_k E\{xx_k\}\right)^2 - \Omega\hat{\Omega} \\ &= 4\left(\sum_k f_k E\{xx_k\}\right)^2. \end{aligned} \tag{17}$$

C. Sinc Interpolator

Several interpolation methods have been proposed for PSAM, including low-pass sinc interpolation [7], Cavers' optimal Wiener interpolator [8], and low-order Gaussian interpolation [9]. In [7], the authors show that for the same PSAM parameters (K and L) and channel characteristics ($\overline{\gamma_b}$ and f_dT_s) that we use in our study, the sinc interpolator achieves nearly the same BER performance as Cavers' optimal Wiener interpolator but with much less complexity. Therefore, we use sinc interpolation in our calculations and simulations for its simplicity and near-optimum performance. The interpolation coefficients f_k^l are computed from the sinc function

$$f_k^l = \mathrm{sinc}\left(\frac{l}{L} - k\right) \tag{20}$$

where $k = -\lfloor (K-1)/2 \rfloor, \cdots, \lfloor K/2 \rfloor$ and $l = 1, \cdots, L-1$. A Hamming window is applied to the sinc function to smooth the abrupt truncation of rectangular windowing.

IV. BER Performance

We first consider the effect of amplitude estimation error on the average BER performance of M-QAM over Rayleigh fading channels. The analysis is then extended to include the effects of both amplitude and phase estimation errors. We compute the BER numerically, based on our analysis for particular PSAM and channel parameters, and compare these results with computer simulation results.

A. Amplitude Estimation Error

1) Conditional BER: Consider first 16-QAM. For each bit stream, the received signal is $r = s\alpha e^{j\theta} + n$, where $s \in \{-3d, -d, d, 3d\}$, $\alpha e^{j\theta}$ is the fading, and n is the noise with variance $\sigma_n^2 = (N_o/2)$. Given the fading amplitude estimate $\hat{\alpha}$ and perfect phase estimation $\hat{\theta} = \theta$, the input to the decision device after scaling by the AGC is then

$$r_d = s\frac{\alpha}{\hat{\alpha}} + \frac{n}{\hat{\alpha}}. \tag{21}$$

We calculate the conditional BER bit by bit for the inphase signal component as shown in Fig. 5. By symmetry, the BER for the quadrature component will be the same. Take the MSB as an example. A bit error occurs when the signal representing bit 1, i.e., $s(\alpha/\hat{\alpha})$, $s = -3d, -d$, falls into the decision boundaries of bit 0, and vice versa. From (21), the noise standard deviation is $\sigma_n/\hat{\alpha}$. Therefore, the bit-error probability of the MSB conditioned on α and $\hat{\alpha}$ is

$$\begin{aligned}P_1(E \mid \alpha, \hat{\alpha}) &= \frac{1}{2}Q\left(\frac{3d\frac{\alpha}{\hat{\alpha}}}{\frac{\sigma_n}{\hat{\alpha}}}\right) + \frac{1}{2}Q\left(\frac{d\frac{\alpha}{\hat{\alpha}}}{\frac{\sigma_n}{\hat{\alpha}}}\right) \\ &= \frac{1}{2}Q\left(\frac{3d\alpha}{\sigma_n}\right) + \frac{1}{2}Q\left(\frac{d\alpha}{\sigma_n}\right).\end{aligned} \tag{22}$$

Similarly, the conditional bit-error probability of the LSB is given by[1]

$$\begin{aligned}P_2(E \mid \alpha, \hat{\alpha}) = &\frac{1}{2}\left[Q\left(\frac{3d\frac{\alpha}{\hat{\alpha}} - 2d}{\frac{\sigma_n}{\hat{\alpha}}}\right) - Q\left(\frac{3d\frac{\alpha}{\hat{\alpha}} + 2d}{\frac{\sigma_n}{\hat{\alpha}}}\right)\right] \\ &+ \frac{1}{2}\left[Q\left(\frac{-d\frac{\alpha}{\hat{\alpha}} + 2d}{\frac{\sigma_n}{\hat{\alpha}}}\right) + Q\left(\frac{d\frac{\alpha}{\hat{\alpha}} + 2d}{\frac{\sigma_n}{\hat{\alpha}}}\right)\right].\end{aligned} \tag{23}$$

Since each bit is mapped to the MSB or the LSB with equal probability, and the error probabilities for the inphase and quadrature components are the same, the average BER conditioned on α and $\hat{\alpha}$ is thus

$$\begin{aligned}P(E \mid \alpha, \hat{\alpha}) &= \frac{1}{2}\left[P_1(E \mid \alpha, \hat{\alpha}) + P_2(E \mid \alpha, \hat{\alpha})\right] \\ &= \frac{1}{4}Q\left(\frac{3\,d\alpha}{\sigma_n}\right) + \frac{1}{4}Q\left(\frac{d\alpha}{\sigma_n}\right) \\ &\quad + \frac{1}{4}Q\left(\frac{3\,d\alpha - 2d\hat{\alpha}}{\sigma_n}\right) - \frac{1}{4}Q\left(\frac{3d\alpha + 2d\hat{\alpha}}{\sigma_n}\right) \\ &\quad + \frac{1}{4}Q\left(\frac{-d\alpha + 2d\hat{\alpha}}{\sigma_n}\right) + \frac{1}{4}Q\left(\frac{d\alpha + 2d\hat{\alpha}}{\sigma_n}\right).\end{aligned} \tag{24}$$

2) Average BER: The BER of 16-QAM is obtained by averaging the conditional BER over the joint distribution given in (5)

$$P_{16\mathrm{QAM}}(E) = \int_0^\infty \int_0^\infty P(E \mid \alpha, \hat{\alpha}) p(\alpha, \hat{\alpha})\, d\alpha\, d\hat{\alpha}. \tag{25}$$

Note that the conditional probability in (24) is a weighted sum of $Q(a\alpha + b\hat{\alpha})$, with a and b being integer multiples of d/σ_n. Define integral $\mathcal{I}(a, b, \Omega, \hat{\Omega}, \rho)$ as

$$\mathcal{I}(a, b, \Omega, \hat{\Omega}, \rho) = \int_0^\infty \int_0^\infty Q(a\alpha + b\hat{\alpha}) p(\alpha, \hat{\alpha})\, d\alpha\, d\hat{\alpha}. \tag{26}$$

Make the following change of variables: $\alpha = \sqrt{\Omega(1-\rho)}r \cos\theta$, $\hat{\alpha} = \sqrt{\hat{\Omega}(1-\rho)}r \sin\theta$, $0 \le r < \infty, 0 \le \theta \le (\pi/2)$. The corresponding Jacobian transformation is

$$J = \frac{\partial(\alpha, \hat{\alpha})}{\partial(r, \theta)} = \sqrt{\Omega\hat{\Omega}}(1-\rho)r. \tag{27}$$

Then $\mathcal{I}(a, b, \Omega, \hat{\Omega}, \rho)$ becomes

$$\begin{aligned}\mathcal{I}(a, b, \Omega, \hat{\Omega}, \rho) = &\int_0^{(\pi/2)} \int_0^\infty 2(1-\rho)Q(cr)r^2 \sin(2\theta) I_0 \\ &\cdot (\sqrt{\rho}\sin(2\theta)r^2) e^{-r^2}\, r\, dr\, d\theta\end{aligned} \tag{28}$$

where $c = \sqrt{\Omega(1-\rho)}a\cos\theta + \sqrt{\hat{\Omega}(1-\rho)}b\sin\theta$.

Defining

$$\mathcal{J}_2(a, b) = a^2 \int_0^\infty e^{-at} t Q(b\sqrt{t})\, dt \tag{29}$$

and using integration by parts, it can be shown that

$$\mathcal{J}_2(a, b) = \frac{1}{2} - \frac{3b}{4\sqrt{2a + b^2}} + \frac{b^3}{4(2a + b^2)^{3/2}}. \tag{30}$$

[1]The $2d$ terms in this expression are not multiplied by $(\alpha/\hat{\alpha})$, since only the received signal is scaled, not the decision boundary. This is equivalent to scaling the boundary and keeping the received signal unchanged.

TABLE II
COEFFICIENTS IN THE BER OF 16-QAM (AMPLITUDE ERROR ONLY)

i	$w_i =$	$a_i =$	$b_i =$
	$\frac{1}{4}\times$	$\frac{1}{\sqrt{5}}\times$	$\frac{1}{\sqrt{5}}\times$
1	1	3	0
2	1	1	0
3	1	3	-2
4	-1	3	2
5	1	-1	2
6	1	1	2

Now setting $t = r^2$ and using the following integral representation of $I_0(z)$ [15]

$$I_0(z) = \frac{1}{\pi}\int_{-(\pi/2)}^{(\pi/2)} e^{-z\sin\phi}\, d\phi \tag{31}$$

we get that $\mathcal{I}(a, b, \Omega, \hat{\Omega}, \rho)$ can be written as (32), shown at the bottom of the page. The average symbol energy of 16-QAM is

$$E_s = 10d^2. \tag{33}$$

Thus

$$\frac{d}{\sigma_n} = \frac{\sqrt{\frac{E_s}{10}}}{\sqrt{\frac{N_o}{2}}} = \frac{\sqrt{\bar{\gamma}}}{\sqrt{5\Omega}} \tag{34}$$

where $\bar{\gamma} = ((\Omega E_s)/N_o)$ is the average SNR per symbol. So, after factoring out Ω, $\mathcal{I}(a, b, \Omega, \hat{\Omega}, \rho)$ can be rewritten in terms of $\bar{\gamma}$ and $r = (\hat{\Omega}/\Omega)$ as in (35), shown at the bottom of the page. Therefore

$$P_{16\text{QAM}}(E) = \sum_{i=1}^{6} w_i \mathcal{I}(a_i, b_i, \bar{\gamma}, r, \rho) \tag{36}$$

where the coefficients w_i, a_i, and b_i are listed in Table II.

3) Higher Level M-QAM: The BER of higher level M-QAM can be calculated in a similar way, which will result in more terms in the summation. Fig. 6 shows the demodulation of 64-QAM bit by bit. Following a similar derivation as in 16-QAM, we obtain the final BER expression

$$P_{64\text{QAM}}(E) = \sum_{i=1}^{28} w_i \mathcal{I}(a_i, b_i, \bar{\gamma}, r, \rho) \tag{37}$$

where the coefficients w_i, a_i, and b_i are listed in Table III.

TABLE III
COEFFICIENTS IN THE BER OF 64-QAM (AMPLITUDE ERROR ONLY)

i	$w_i =$	$a_i =$	$b_i =$	i	$w_i =$	$a_i =$	$b_i =$	i	$w_i =$	$a_i =$	$b_i =$
	$\frac{1}{12}\times$	$\frac{1}{\sqrt{42}}\times$	$\frac{1}{\sqrt{42}}\times$		$\frac{1}{12}\times$	$\frac{1}{\sqrt{42}}\times$	$\frac{1}{\sqrt{42}}\times$		$\frac{1}{12}\times$	$\frac{1}{\sqrt{42}}\times$	$\frac{1}{\sqrt{42}}\times$
1	1	1	0	11	1	-1	4	21	1	-3	3
2	1	3	0	12	1	1	4	22	1	3	1
3	1	5	0	13	1	7	-6	23	-1	3	5
4	1	7	0	14	-1	7	-2	24	1	3	9
5	1	7	-4	15	1	7	2	25	1	-1	1
6	-1	7	4	16	-1	7	6	26	-1	-1	5
7	1	5	-4	17	1	-5	6	27	1	1	3
8	-1	5	4	18	1	5	-2	28	1	-1	7
9	1	-3	4	19	-1	5	2				
10	1	3	4	20	1	5	6				

B. Amplitude and Phase Estimation Error

From (6), we can derive the pdf of the phase estimation error ψ, $\psi = \theta - \hat{\theta}$, to be

$$p(\psi) = \frac{1-\rho}{4\pi^2}\left[\frac{(1-q^2)^{1/2} + q(\pi - \cos^{-1} q)}{(1-q^2)^{3/2}}\right](2\pi - |\psi|), \quad -2\pi \le \psi \le 2\pi \tag{38}$$

where $q = \sqrt{\rho}\cos\psi$. With the phase error, I and Q channels interfere with each other, and (21) becomes

$$r_d = (s_I \cos\psi + s_Q \sin\psi)\frac{\alpha}{\hat{\alpha}} + \frac{n}{\hat{\alpha}} \tag{39}$$

where s_I and s_Q are the inphase and quadrature components of the complex signal mapping. For 16-QAM, $s_I, s_Q \in \{-3d, -d, d, 3d\}$. The conditional error probability in (24) is therefore conditioned further on ψ and s_Q. However, only positive values of s_Q need to be considered due to symmetry. Taking the above into account, (35) becomes

$$\begin{aligned}\mathcal{I}&(a_1, a_2, b, \bar{\gamma}, r, \rho)\\ &= \frac{1-\rho}{\pi}\int_{-2\pi}^{2\pi}\int_0^{(\pi/2)}\int_{-(\pi/2)}^{(\pi/2)} \frac{\sin 2\theta p(\psi)}{(\sqrt{\rho}\sin 2\theta\sin\phi + 1)^2}\\ &\quad \cdot \mathcal{J}_2\Big(\sqrt{\rho}\sin 2\theta \sin\phi + 1, \sqrt{(1-\rho)\bar{\gamma}}\\ &\quad \cdot \big((a_1\cos\psi + a_2\sin\psi)\cos\theta + \sqrt{r}b\sin\theta\big)\Big)\, d\phi\, d\theta\, d\psi.\end{aligned} \tag{40}$$

Thus (36) becomes

$$P_{16\text{QAM}}(E) = \sum_{i=1}^{12} w_i \mathcal{I}(a_{1i}, a_{2i}, b_i, \bar{\gamma}, r, \rho) \tag{41}$$

$$\mathcal{I}(a, b, \Omega, \hat{\Omega}, \rho) = \frac{1-\rho}{\pi}\int_0^{\pi/2}\int_{-\pi/2}^{\pi/2} \frac{\sin 2\theta \mathcal{J}_2\Big(\sqrt{\rho}\sin 2\theta\sin\phi + 1, \sqrt{1-\rho}\Big(a\sqrt{\Omega}\cos\theta + b\sqrt{\hat{\Omega}}\sin\theta\Big)\Big)}{(\sqrt{\rho}\sin 2\theta \sin\phi + 1)^2}\, d\phi\, d\theta \tag{32}$$

$$\mathcal{I}(a, b, \bar{\gamma}, r, \rho) = \frac{1-\rho}{\pi}\int_0^{\pi/2}\int_{-\pi/2}^{\pi/2} \frac{\sin 2\theta \mathcal{J}_2\Big(\sqrt{\rho}\sin 2\theta\sin\phi + 1, \sqrt{(1-\rho)\bar{\gamma}}(a\cos\theta + \sqrt{r}b\sin\theta)\Big)}{(\sqrt{\rho}\sin 2\theta\sin\phi + 1)^2}\, d\phi\, d\theta \tag{35}$$

TABLE IV
COEFFICIENTS IN THE BER OF 16-QAM (AMPLITUDE AND PHASE ERROR)

i	$w_i =$	$a_{1i} =$	$a_{2i} =$	$b_i =$	i	$w_i =$	$a_{1i} =$	$a_{2i} =$	$b_i =$
	$\frac{1}{8}\times$	$\frac{1}{\sqrt{5}}\times$	$\frac{1}{\sqrt{5}}\times$	$\frac{1}{\sqrt{5}}\times$		$\frac{1}{8}\times$	$\frac{1}{\sqrt{5}}\times$	$\frac{1}{\sqrt{5}}\times$	$\frac{1}{\sqrt{5}}\times$
1	1	3	1	0	7	-1	3	1	2
2	1	3	3	0	8	-1	3	3	2
3	1	1	1	0	9	1	-1	1	2
4	1	1	3	0	10	1	-1	3	2
5	1	3	1	-2	11	1	1	1	2
6	1	3	3	-2	12	1	1	3	2

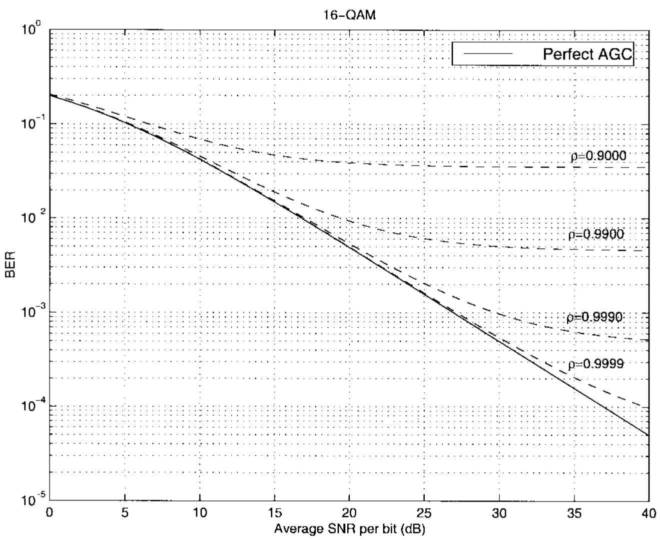

Fig. 9. 16-QAM BER performance. $r = 1$.

where the coefficients w_i, a_{1i}, a_{2i}, and b_i are listed in Table IV.

C. Numerical and Simulation Examples

Figs. 9 and 10 show the effect of the amplitude estimation error as a function of the correlation coefficient ρ on the BER of 16-QAM and 64-QAM, respectively, with $r = (\hat{\Omega}/\Omega)$ fixed at 1.[2] These figures indicate that an error floor occurs as ρ decreases from 1. This result is expected, since as ρ decreases from 1, the fading estimate and the corresponding AGC exhibit increasing error. Equivalently, the decision regions for demodulation are increasingly offset, which can lead to errors even in the absence of noise, i.e., an error floor. Note that ρ, given by (18), is a function of $\overline{\gamma_b}$, K, L, and f_dT_s. Thus, the values of these parameters must be chosen so that ρ is sufficiently close to 1 in order to meet the BER target. In Table V, we compute ρ from (18) for a range of $\overline{\gamma_b}$, K, L, and f_dT_s values. As expected, ρ increases toward 1 as the average SNR per bit $(\overline{\gamma_b})$ and the interpolation size for the PSAM estimate (K) increase, and as the frame size (L) decreases. ρ will also increase as the normalized Doppler f_DT_s decreases.

Figs. 11 and 12 show the BER performance of 16-QAM and 64-QAM, respectively, as a function of the average SNR per bit $\overline{\gamma_b}$. From Table V, we see that for the parameters used in these calculations, for 16-QAM, ρ is equal to 0.93 at $\overline{\gamma_b} = 5$ dB, 0.9976 at $\overline{\gamma_b} = 20$ dB, and 0.999 91 at $\overline{\gamma_b} = 35$ dB. For 64-QAM, ρ is equal to 0.95 at $\overline{\gamma_b} = 5$ dB, 0.9984 at $\overline{\gamma_b} = 20$ dB, and 0.999 94 at $\overline{\gamma_b} = 35$ dB. Thus, Figs. 11 and 12 exhibit no error floor, since we see from Figs. 9 and 10 that these values of ρ are sufficiently close to 1 at each $\overline{\gamma_b}$ to avoid this floor. Figs. 11 and 12 indicate that amplitude

[2]For practical values of $\overline{\gamma_b}$, K, L, and f_dT_s, r is very close to 1 and has little effect on BER.

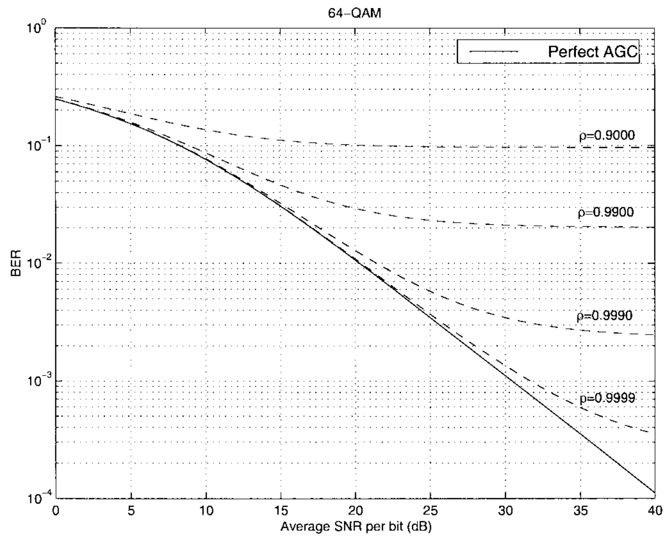

Fig. 10. 64-QAM BER performance. $r = 1$.

TABLE V
VALUES OF r AND ρ FOR $f_dT_s = 0.03$

$\overline{\gamma_b}$ (dB)	K	L	16-QAM		64-QAM	
			r	ρ	r	ρ
5	30	15	1.0758	0.92855	1.0502	0.95120
20	30	15	1.0014	0.99756	1.0006	0.99837
20	15	15	0.9521	0.99186	0.9513	0.99268
20	30	5	1.0028	0.99759	1.0020	0.99839
35	30	15	0.9990	0.99991	0.9990	0.99994

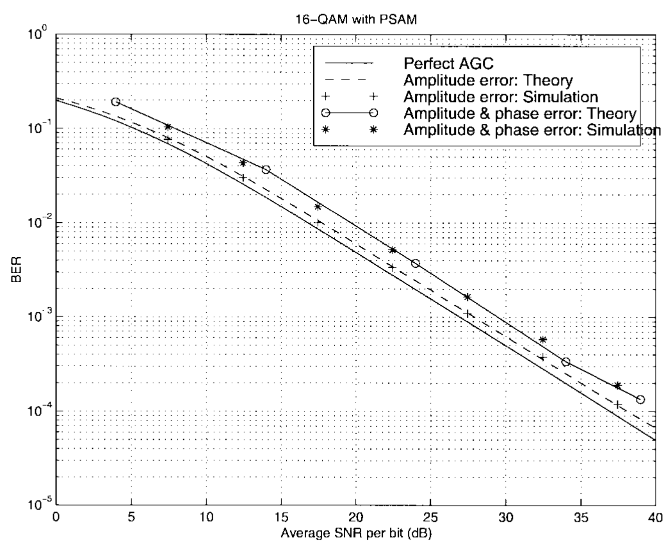

Fig. 11. BER of 16-QAM with PSAM. $L = 15$, $K = 30$, and $f_dT_s = 0.03$.

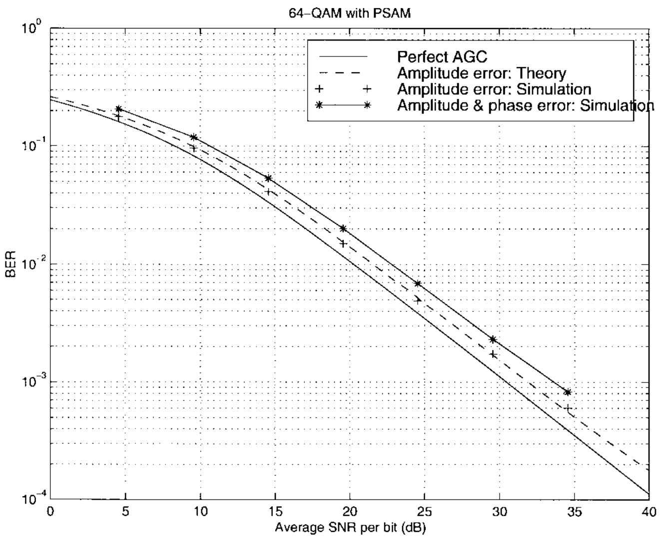

Fig. 12. BER of 64-QAM with PSAM. $L = 15$, $K = 30$, and $f_d T_s = 0.03$.

estimation error leads to a 1-dB degradation in $\overline{\gamma_b}$, as shown in the dashed line, and that combined amplitude and phase error leads to a 2.5-dB degradation, as shown by stars, for the parameters we use. Computer simulations were also done to verify the analytical results. The simulation followed the system block diagram in Fig. 1, except that the pulse shaping and the matched filter were omitted since we assumed matched filtering with zero intersymbol interference and perfect symbol timing at the receiver. The Rayleigh fading was simulated using the model described in [14, Sec. 2.3.2]. Simulation results closely match the analysis. Note that power loss due to insertion of the pilot symbols ($10 \log(L/(L-1))$ dB) is not factored into the calculations for Figs. 11 and 12, but it is easily included by appropriate scaling of the x-axis.

V. Conclusion

We have studied the effect of fading amplitude and phase estimation error on the BER of 16-QAM and 64-QAM with PSAM over flat Rayleigh fading channels. The results are obtained by averaging the conditional BER over the joint distribution of the fading and its estimate. The exact BER expressions are given by finite-range integrals as a function of the PSAM parameters. We find that for 16-QAM and 64-QAM, amplitude estimation error yields approximately 1 dB of degradation in average SNR, and combined amplitude-phase estimation error yields a 2.5-dB degradation for the system parameters we considered. Our results allow the designers of M-QAM with PSAM to easily choose system parameters to meet their performance requirements under reasonable channel Doppler conditions.

Acknowledgment

The authors gratefully acknowledge L. Greenstein for many useful discussions and suggestions. They would also like to thank the anonymous reviewers for their careful reading and critique of the manuscript. Their suggestions greatly improved its clarity.

References

[1] P. M. Fortune, L. Hanzo, and R. Steele, “On the computation of 16-QAM and 64-QAM performance in Rayleigh-fading channels,” *Inst. Electron. Commun. Eng. Trans. Commun.*, vol. E75-B, pp. 466–475, June 1992.
[2] L. Hanzo, R. Steele, and P. Fortune, “A subband coding, BCH coding and 16QAM system for mobile radio speech communications,” *IEEE Trans. Veh. Technol.*, vol. 39, pp. 327–339, Nov. 1990.
[3] N. Kinoshita, S. Sampei, E. Moriyama, H. Sasaoka, Y. Kamio, K. Hiramatsu, K. Miya, K. Inogai, and K. Homma, “Field experiments on 16QAM/TDMA and trellis coded 16QAM/TDMA systems for digital land mobile radio communications,” *Inst. Electron. Commun. Eng. Trans. Commun.*, vol. E77-B, pp. 911–920, July 1994.
[4] W. T. Webb and R. Steele, “Variable rate QAM for mobile radio,” *IEEE Trans. Commun.*, vol. 43, pp. 2223–2230, July 1995.
[5] A. Goldsmith and S. G. Chua, “Variable-rate variable-power M-QAM for fading channels,” *IEEE Trans. Commun.*, vol. 45, pp. 1218–1230, Oct. 1997.
[6] W. T. Webb and L. Hanzo, *Modern Quadrature Amplitude Modulation*. New York, IEEE Press, 1994.
[7] Y. S. Kim, C. J. Kim, G. Y. Jeong, Y. J. Bang, H. K. Park, and S. S. Choi, “New Rayleigh fading channel estimator based on PSAM channel sounding technique,” in *Proc. IEEE Int. Conf. Commun. (ICC)*, Montreal, Canada, June 1997, pp. 1518–1520.
[8] J. K. Cavers, “An analysis of pilot symbol assisted modulation for Rayleigh fading channels,” *IEEE Trans. Veh. Technol.*, vol. 40, pp. 686–693, Nov. 1991.
[9] S. Sampei and T. Sunaga, “Rayleigh fading compensation for QAM in land mobile radio communications,” *IEEE Trans. Veh. Technol.*, vol. 42, pp. 137–147, May 1993.
[10] J. M. Torrance and L. Hanzo, “Comparative study of pilot symbol assisted modem schemes,” in *Proc. Radio Receivers and Associated Systems Conf. (RRAS)*, Bath, U.K., Sept. 1995, pp. 36–41.
[11] T. L. Staley, R. C. North, W. H. Ju, and J. R. Zeidler, “Channel estimate-based error probability performance prediction for multichannel reception of linearly modulated coherent systems on fading channels,” in *Proc. IEEE Military Commun. Conf. (MILCOM)*, McLean, VA, Oct. 1996.
[12] M. G. Shayesteh and A. Aghamohammadi, “On the error probability of linearly modulated signals on frequency-flat Ricean, Rayleigh and AWGN channels,” *IEEE Trans. Commun.*, vol. 43, pp. 1454–1466, Feb./Mar./Apr. 1995.
[13] W. B. Davenport and W. L. Root, *Random Signals and Noise*. New York: McGraw-Hill, 1958.
[14] G. L. Stuber, *Principles of Mobile Communication*. Norwell, MA: Kluwer, 1996.
[15] I. S. Gradshteyn and I. M. Ryzhik, *Table of Integrals, Series, and Products*. New York: Academic, 1980.

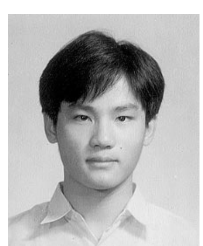

Xiaoyi Tang received the B.S. degree in electrical engineering from the California Institute of Technology in 1999. Currently, he is a graduate student in electrical engineering at the University of California, Berkeley, CA.

Mr. Tang is a recipient of the Caltech Summer Undergraduate Fellowship (SURF) Award and a Caltech Merit Award.

Mohamed-Slim Alouini (S’94–M’99), for a photograph and biography, see p. 43 of the January 1999 issue of this Transactions.

Andrea J. Goldsmith (S’94–M’95–SM’99), for a photograph and biography, see p. 1334 of the September 1999 issue of this Transactions.